CHEMBIOCHEM

Supporting Information

© Copyright Wiley-VCH Verlag GmbH & Co. KGaA, 69451 Weinheim, 2013

Carnosine Inhibits $A\beta_{42}$ Aggregation by Perturbing the H-Bond Network in and around the Central Hydrophobic Cluster

Francesco Attanasio,[a] Marino Convertino,[b] Andrea Magno,[b] Amedeo Caflisch,[b] Alessandra Corazza,[c] Haritha Haridas,[c] Gennaro Esposito,[c] Sebastiano Cataldo,[d] Bruno Pignataro,[d] Danilo Milardi,*[a] and Enrico Rizzarelli[a, e]

cbic_201200704_sm_miscellaneous_information.pdf

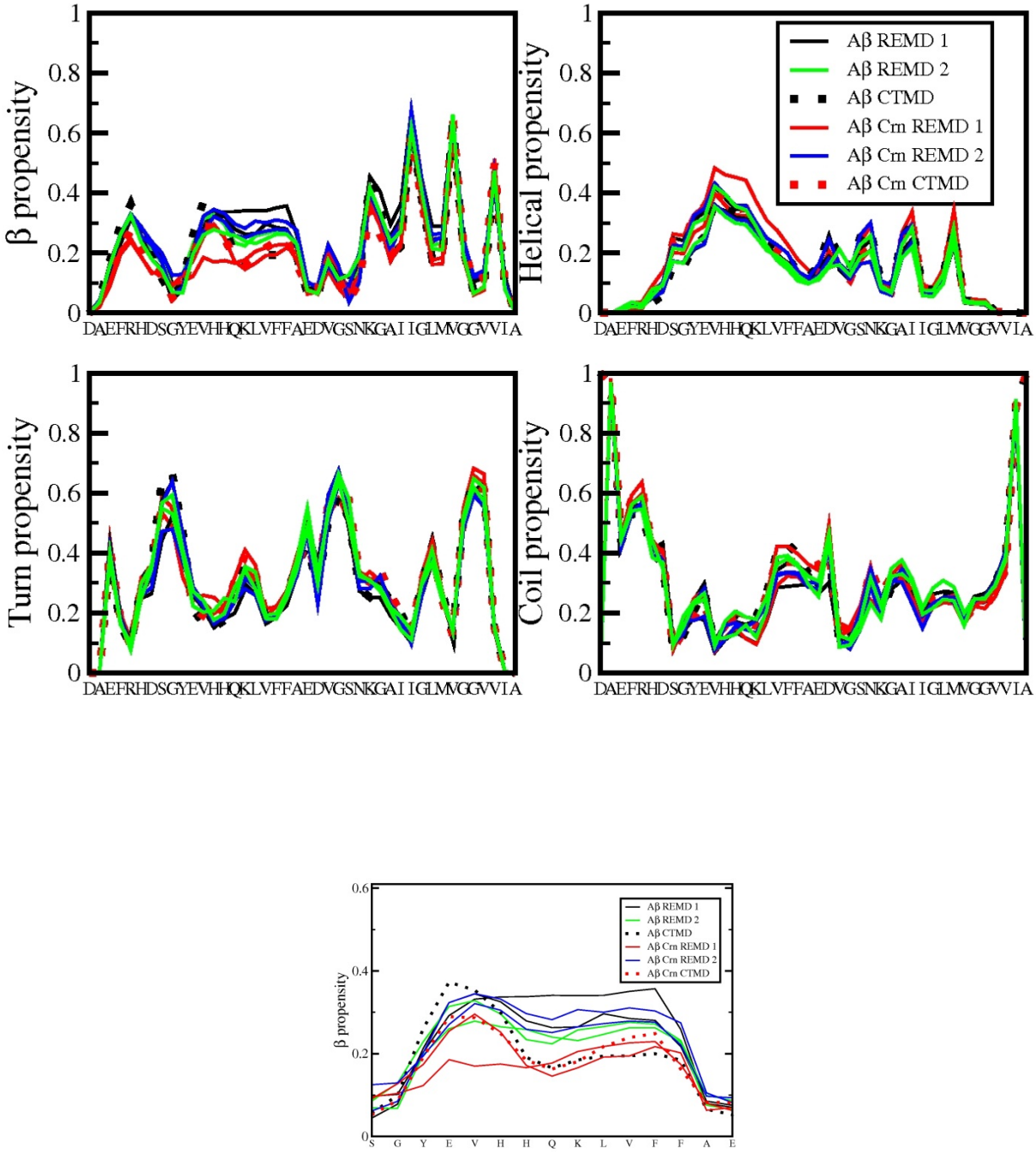

Figure S1. Secondary structure propensities along the Aβ42 sequence at T = 300K, with and without carnosine. For each system, two independent simulations have been performed with the REMD technique (solid lines). Moreover, a constant temperature molecular dynamics (CTMD, dashed lines) simulation has been run at 300 K to increase confidence in the statistical robustness of the results. The panel in the bottom shows an enlargement of the profile with the highest statistical noise which is the β-propensity of the segment from Ser8 to Glu22.

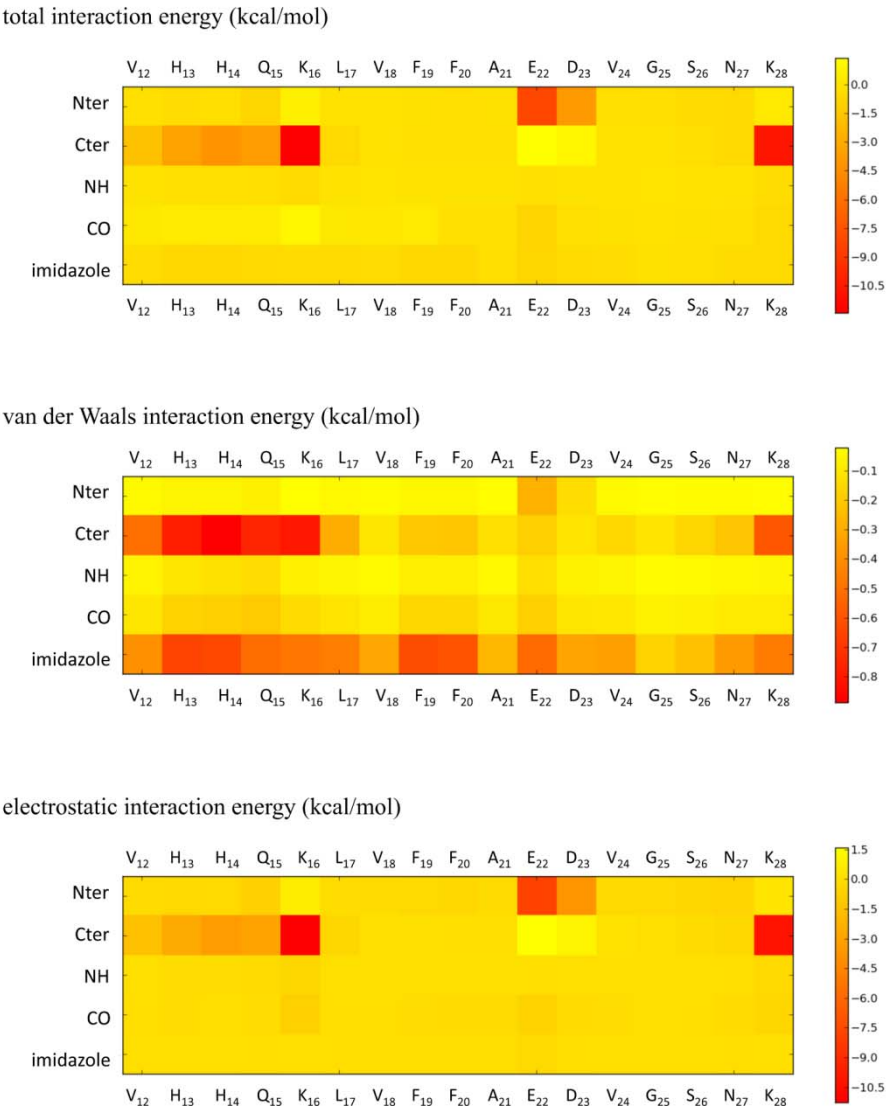

Figure S2. Interaction energy matrix for carnosine and monomeric Aβ12-28. Each colored square shows the interaction energy between a single functional group of carnosine and a single Aβ12-28 residue (backbone and side chain atoms) averaged over the whole 15 microsecond sampling. The decomposition of intermolecular energy into contributions of individual pairs of functional groups illustrates that the main interactions involve formal charges of opposite sign, i.e., the N-terminal amino group of carnosine with the E22 and D23 side chains, and the C-terminal carboxy group of carnosine with the K16 and K28 side chains. Although the electrostatic contribution seems to dominate, one has to underline that desolvation effects are not taken into account in the interaction energy matrix. The electrostatic desolvation of charged groups is unfavorable and does significantly counter-balance the favorable electrostatic interactions between the termini of carnosine and the charged side chains of Aβ. There are also favorable van der Waals interactions involving the imidazole ring of carnosine with mainly the aromatic side chains of Aβ but also other Aβ residues, as well as the carboxy group of carnosine and the Aβ12-16 segment.

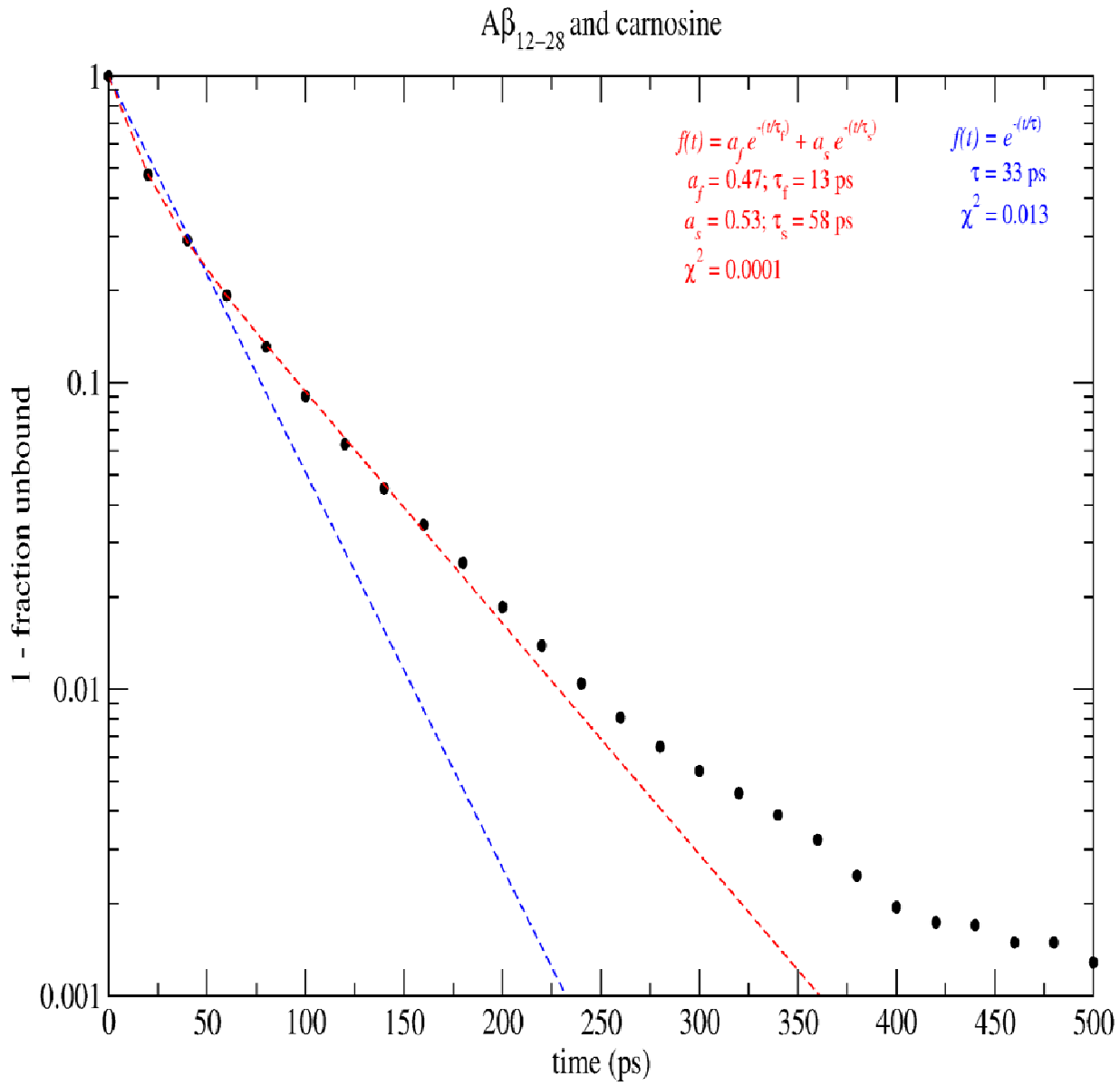

Figure S3. Cumulative distribution of the time of carnosine unbinding from Aβ12-28 extracted from the MD trajectories (filled circles). The kinetics of unbinding show a negligible dependence of the energy threshold used to define a binding event in the range from -20 to 0 kcal/mol. The cumulative distribution of the time of unbinding of carnosine from Aβ12-28 can be fitted by a double-exponential (red dashed line and legend) with similar amplitude for the slow and fast phase. This result and the characteristic time of only 58 ps for the slow phase indicate that the intermolecular interactions are transient (fast unbinding). The transient nature of the association of carnosine to monomeric Aβ12-28 is consistent with the increase of the hydrodynamic radius (R_h) of carnosine and the minor increase of the R_h of Aβ12-28 as derived from the NMR DOSY measurements. Note that the unbinding times of carnosine represent lower bounds because of the low friction used in the Langevin simulations, and it is likely that the real unbinding times are 10-100 times slower as suggested by previously reported comparisons of implicit solvent simulations with experimental data on peptide folding times (Hiltpold et al. 2000). In any case, even upon correcting for the lack of friction, unbinding time scales of about 0.5 ns to 5 ns still correspond to weak/short lived association.

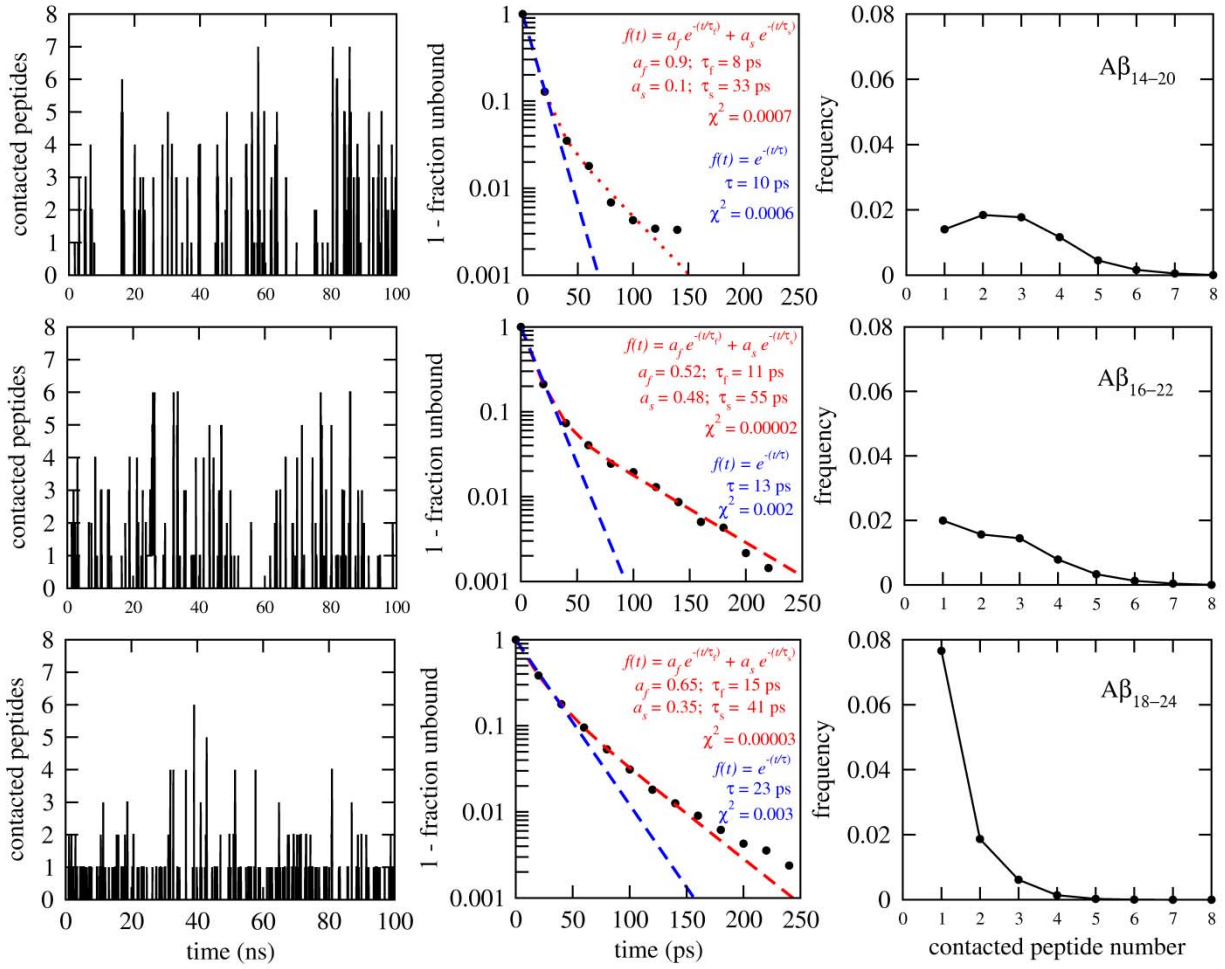

Figure S4. Transient binding of carnosine to oligomers of Aβ14-20 (top), Aβ16-22 (middle), and Aβ18-24 (bottom). The figure shows the time series (left column) and distribution (right column) of the number of Aβ heptapeptides in contact with carnosine. The time series show a trajectory subsegment of only 100 ns for clarity. The distributions are normalized to one by including in the count fully isolated carnosine whose data point (at x=0) is not shown as it lies outside the y-axis range. (Middle column) The cumulative distribution of the time of carnosine unbinding from the Aβ heptapeptide oligomers is shown with fitting curves and parameters in red and blue for double-exponential and single-exponential fitting, respectively. The residence time of carnosine on the oligomeric Aβ heptapeptide systems can be visualized by the time series of the number of Aβ heptapeptides in contact with carnosine (left). The double exponential fitting yields characteristic times of about 10 ps and 50 ps. Visual analysis of the trajectories of Aβ14-20 and Aβ16-22 indicates that the slow phase originates from carnosine dissociation from aggregates with significant intermolecular β-sheet structure, with which carnosine is involved in multiple transient interactions.

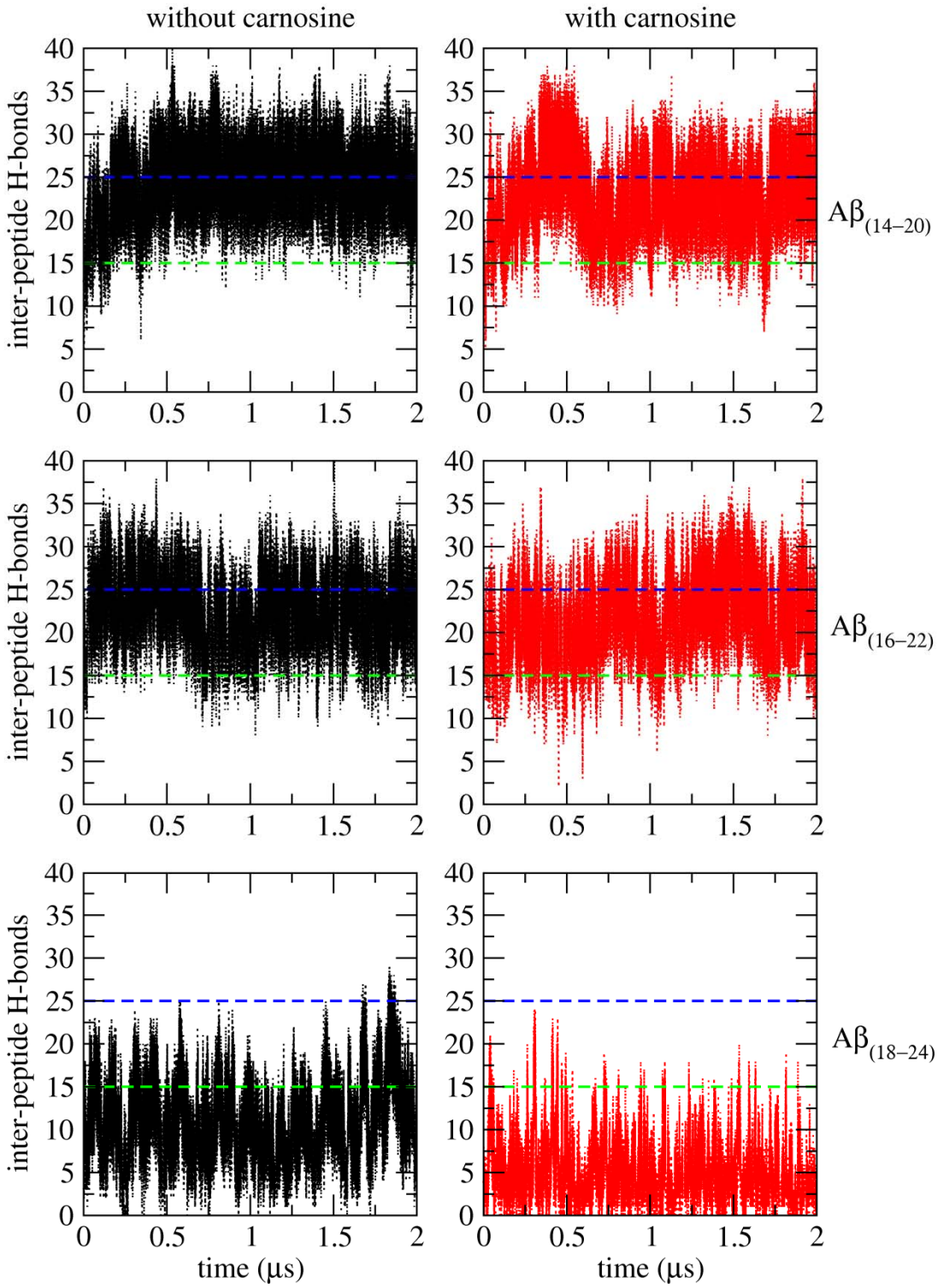

Figure S5. Time series of number of inter-peptide backbone hydrogen bonds. The horizontal lines at y=15 and y=25 are drawn to facilitate the comparison of the different plots.

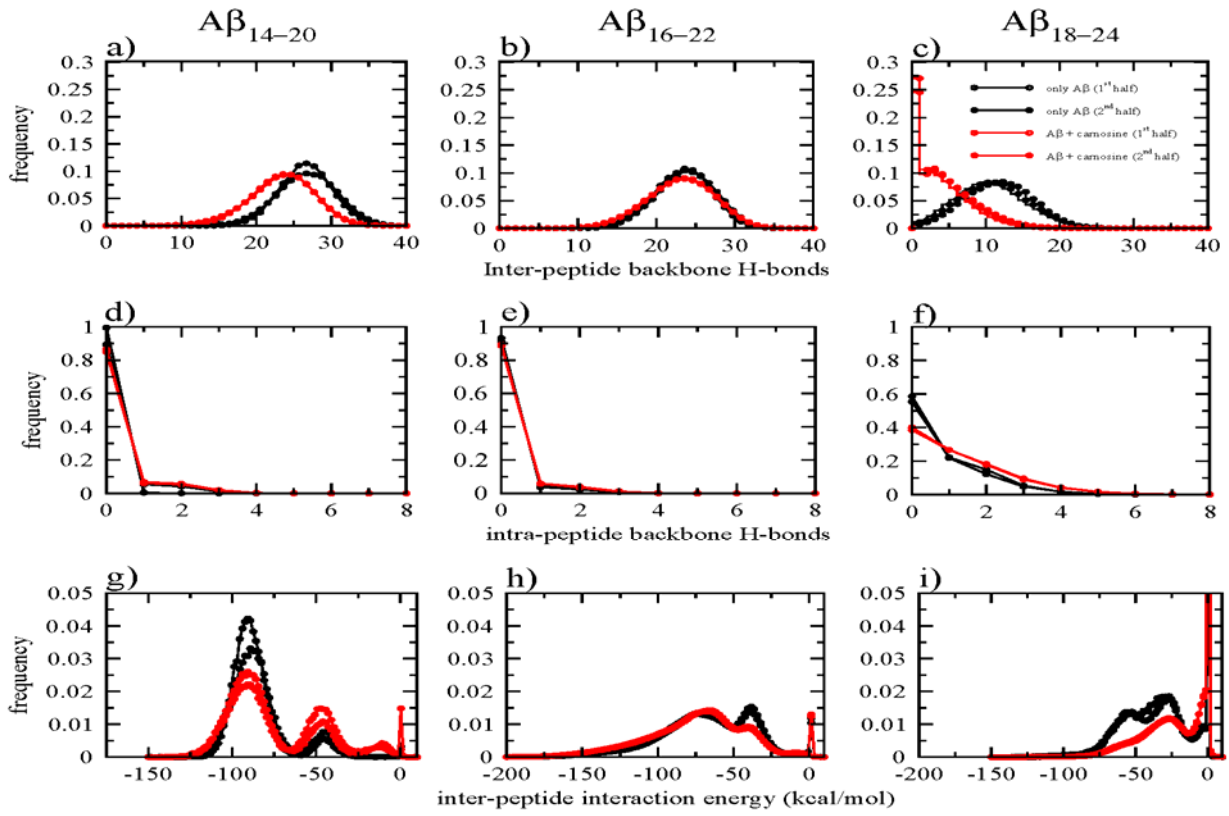

Figure S6. Distributions of number of intermolecular hydrogen bonds (top), intramolecular hydrogen bonds (middle), and intermolecular energy (bottom). For each system, block averaging was carried out by dividing the total sampling of 20 μs (ten 2-μs runs) into two blocks of 10 μs each (five MD runs). The differences in the presence and absence of carnosine (compare red with black lines) are significantly larger than the statistical noise (compare lines of same color). Moreover, the almost indistinguishable histograms of the two blocks of each system indicate that the statistical error is negligible.

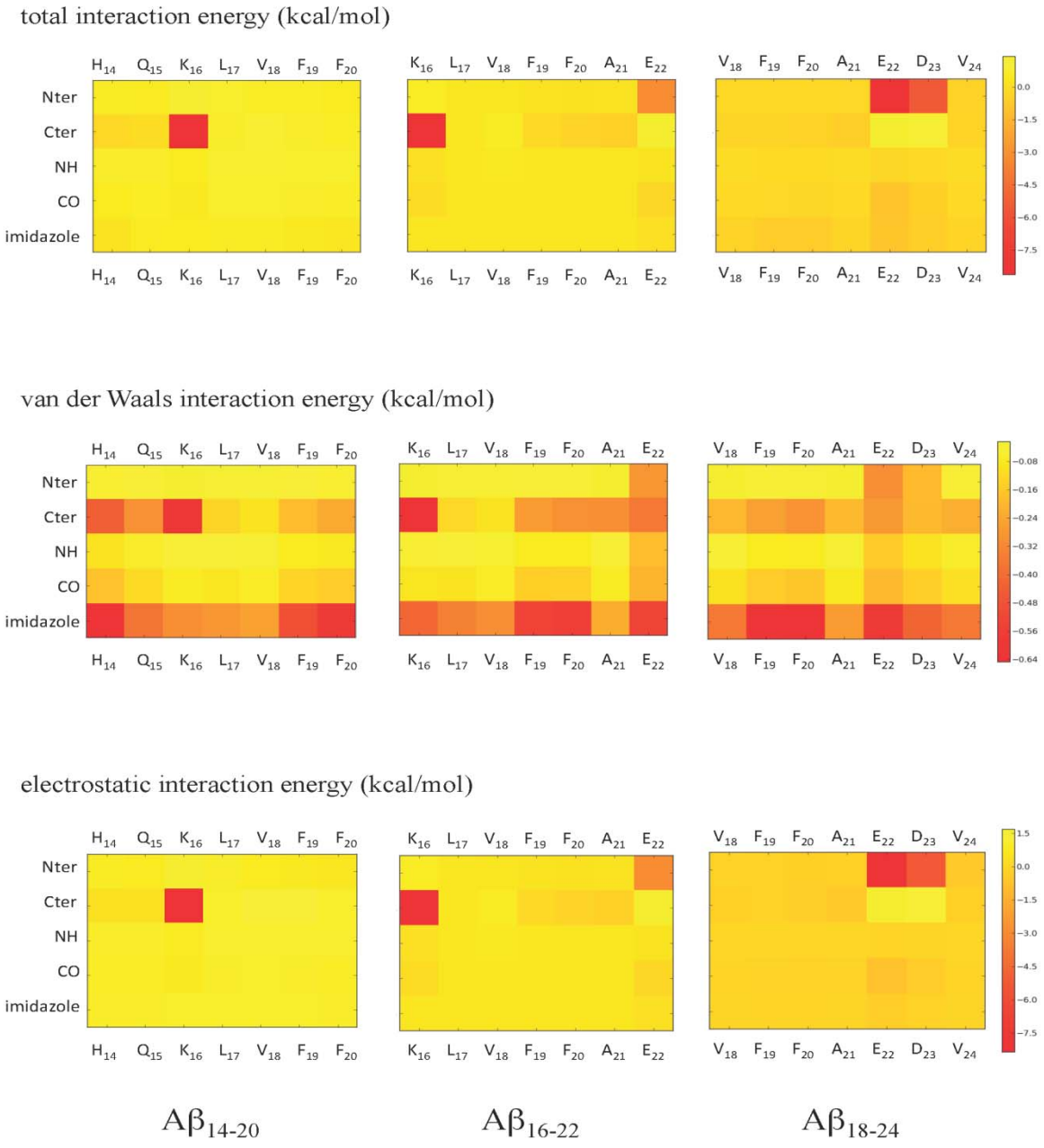

Figure S7. Interaction energy matrix for carnosine and Aβ14-20 (left), Aβ16-22 (middle), and Aβ18-24 (right).

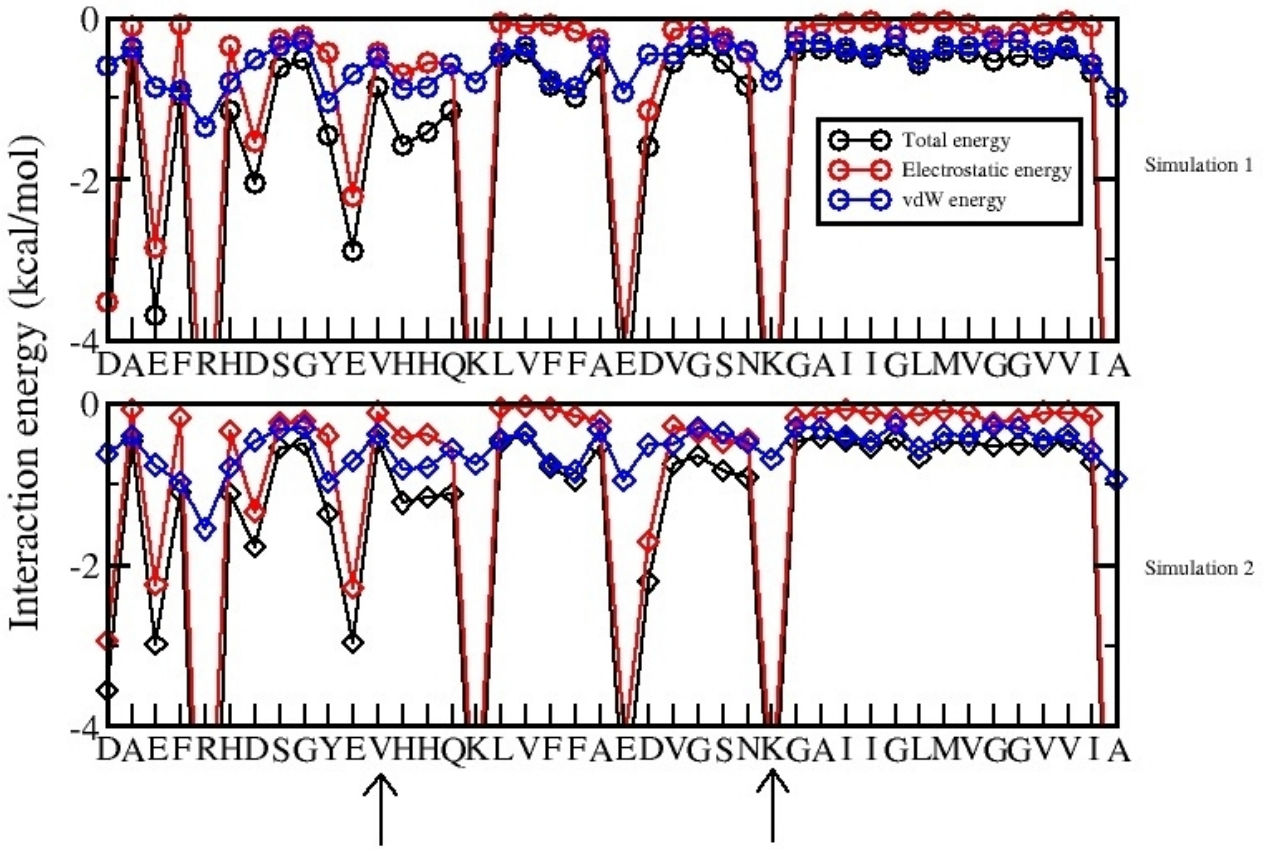

Figure S8. The 300 K interaction energy profiles of carnosine with Aβ42 plotted separately for the two REMD runs show that these data are converged. The two vertical arrows emphasize the segment Aβ12-28 used in the NMR experiments.

References

Hiltpold et al. *J. Phys. Chem. B* 2000, **104**, 10080-10086.